A lab-on-a-chip model of glaucoma

Fatemeh Nafian,†[a] Babak Kamali Doust Azad,†[b] Shahin Yazdani [c,d], Mohammad Javad Rasaee,*[a] and Narsis Daftarian *[c,d]

[a] Department of Medical Biotechnology, Faculty of Medical Sciences, Tarbiat Modares University, Tehran, Iran.

[b] Department of Electronics, School of Electrical and Computer Engineering, Tehran University, Tehran, Iran.

[c] Ocular Tissue Engineering Research Center, Shahid Beheshti University of Medical Sciences, Tehran, Iran.

[d] Ophthalmic Research Center, Shahid Beheshti University of Medical Sciences, Tehran, Iran.

† FN and BKDA has contributed equally to this work and should be considered as co-first authors.

* MJR and ND are co-corresponding authors. All queries and request for reprints should be addressed to MJR.
Email: rasaee_m@modares.ac.ir, Tel: +98-21-82884513; FAX: +98-21-82883858.

Keywords: Glaucoma; Lab-on-a-chip; microenvironment design; elevated hydrostatic pressure; retinal ganglion cell; cell viability.

Summary statement: Glaucoma-on-a-chip offers the advantages of allowing controlled experimental conditions, preliminary targeting of a specific cell type or pathway involved in glaucoma and investigating putative neuroprotective agents prior to assessment in animal models.

Abstract

We developed a glaucoma-on-a-chip (GOC) model to evaluate the viability of retinal ganglion cells (RGCs) against high pressure and neuroprotective treatments. A three-layered chip consisting of interconnecting microchannels and culture wells was fabricated based on simulation of physical parameters. The bottom surface of the wells was mechanically modified by air plasma and coated with different membranes to model an extracellular microenvironment. SH-SY5Y used as model cells to determine the best supporting membrane which was revealed to be PDL/laminin. RGCs were isolated from postnatal Wistar rats and purified by magnetic assisted cell sorting up to 70%. The cultured RGCs were exposed to normal (15 mmHg) or elevated pressure (33 mmHg) for 6, 12, 24, 36 and 48 hours, with and without adding brain-derived-neurotrophic factor (BDNF) or a novel BDNF mimetic (named RNYK). RGC survival rates were 85, 78, 70, 67 and 61% under normal pressure versus 40, 22, 18, 12 and 10% under high pressure at 6, 12, 24, 36 and 48 hours, respectively ($P<0.0001$). BDNF and RNYK reduced the rate of RGC death under both normal and elevated pressures, two-fold approximately ($p<0.01$-0.0001).

Introduction

Glaucoma is a collective term used to define a group of neurodegenerative processes affecting the entire visual pathway best distinguished by progressive, irreversible destruction and death of retinal ganglion cells (RGCs). The disease spectrum is estimated to affect more than 100 million people worldwide by the year of 2040 (Tham et al., 2014). The primary risk factor for progression and development of glaucoma is elevated intraocular pressure (IOP). IOP is regulated by the balance between aqueous humor secretion into the anterior chamber on one hand and its drainage via the trabecular meshwork (conventional outflow) or the uveoscleral outflow pathways on the other hand (Levin et al., 2011). The average value for normal IOP in most population based human studies is 14-17 mmHg with 95% confidence intervals of 10-21 mmHg (Rieck, 2013).

Several experimental in vivo glaucoma models have been developed and used for studies on glaucoma mechanisms. These include laser photocoagulation of the Perilimbal region (Gaasterland and Kupfer, 1974), red blood cell or microbeads injection into the anterior chamber (Kalvin et al., 1966; Quigley and Addicks, 1980), Episcleral vein obstruction (Fedorchak et al., 2014), and Episcleral vein saline injection (Morrison et al., 1997; Shareef et al., 1995; Vecino and Sharma, 2011). Without sequential treatments, the duration of IOP elevation is transient in these models. Precise control over IOP elevation is difficult and certain problems may occur; these include intraocular inflammation, irreversible mydriasis, IOP variability, hyphema, reduced visibility of optic discs, corneal opacity, and scleral burns (Johnson and Tomarev, 2010; Rudzinski and Saragovi, 2005). While in vivo animal models are indispensable to determine what events occur in live organisms, these strategies typically involve poorly defined and uncontrollable factors and the results can be difficult to understand at cellular and molecular levels (Ishikawa et al., 2015).

Ishikawa et al. designed an ex vivo hydrostatic pressure model which demonstrated better retention of neuron-neuron and neuron-glial interactions in dissected eye cups (Ishikawa et al., 2016; Ishikawa et al., 2018; Ishikawa et al., 2010; Ishikawa et al., 2011; Ishikawa et al., 2014). This model excluded the effects of ischemia and allowed

53 studying of the direct effects of pressure on the retina. Eyecups were sunken to the bottom of a glass cylinders
54 containing different liquid heights. Although ex vivo systems produce reliable results, there are several limitations.
55 For example, the incubation period is limited by the duration of tissue viability because survival factors originating
56 from axonal transport or the bloodstream are eliminated in ex vivo models(Ishikawa et al., 2015).

57 To overcome these limitations, in vitro models have been developed using cultured cells in supporting
58 environments to clarify glaucoma mechanisms and appear as valuable tools to evaluate the response of individual
59 cell populations against noxious conditions and novel treatments (Dai et al., 2018; Lei et al., 2011; Maurya et al.,
60 2016). These models have studied optic nerve head astrocytes, RGCs and other types of retinal cells utilizing pressure
61 loading systems (Agar et al., 2006; Hernandez et al., 2000; Lei et al., 2011; Ricard et al., 2000; Salvador-Silva et al.,
62 2004; Tezel and Wax, 2000; Wax et al., 2000; Yang et al., 2004). Elevation of pressure constitutes the gold standard
63 to model ocular hypertension in vitro and has gained increasing attention in recent years. Elevated hydrostatic
64 pressure (EHP) systems provide remarkable information on cell apoptosis, elastin synthesis, cell migration, and
65 production of cell adhesion molecules. EHPs have provided new insights into the molecular and cellular mechanisms
66 of glaucoma.

67 Recently, lab-on-a-chip (LOC) technology has been developed. This approach entails a simpler and smaller
68 analysis platform, resulting in better temporal and spatial control of local cellular microenvironments, passive and
69 active cell handling, less consumption of reagents, faster test results, economizing study logistics and energy savings
70 (Balijepalli and Sivaramakrishan, 2017; El-Ali et al., 2006; Esch et al., 2015; Ingber, 2016). With the goal of
71 transferring costly laboratory equipment onto small, user-friendly, easily replicable chips, LOC technology has
72 dramatically altered many fields such as medicine, biochemistry, and biotechnology.

73 The aim of the present study was to design and establish a glaucoma-on-a-chip (GOC) model consisting of an
74 EHP system, coupled to a microculture system using purified primary rat RGCs. To achieve this aim, we designed
75 pressure chips in which HP could be modulated with the added benefits of higher speed, greater precision and finer
76 control than previous EHP systems. We studied RGC survival under normal versus elevated hydrostatic pressures
77 and also compared survival of these cells when treated with a neuroprotective growth factor (brain-derived
78 neurotrophic factor, BDNF) or a mimicry peptide, named RNYK, as a putative agonist of neurotrophic tyrosine
79 kinase receptor type 2 (NTRK2) (Nafian et al., 2018). BDNF is a well-known neuroprotectant and a potent therapeutic
80 candidate for neurodegenerative diseases. However, there are several clinical concerns about its therapeutic
81 applications. RNYK as a mimicking small peptide (similar to loop2 of BDNF) is an alternative to circumvent these
82 problems. The RNYK neuroprotective effect has been confirmed with equal efficacy to or even better than BDNF.

83 # Results

84 ## Testing of the three-layered chip

85 The three-layered chip was designed to allow inflow of cell culture media from feeding inlets in layer A into the
86 wells in layer B adjacent to layer C which acts the culture surface at the bottom of the wells (Fig. 1). We fabricated

87 stand-alone feeding inlets for each well to let treat culture cells within the wells in an individual manner. We initially
88 devised two feeding ports per well in layer A (the results not shown). The drawback to this design was inappropriate
89 surface tension leading to an uneven distribution of the culture media. We then shifted to a single feeding port at one
90 extreme of the well and placed a gas inlet on the other extreme to allow uniform liquid distribution. Locating the
91 feeding port at the extreme end of the well reduced shearing stress and avoided cellular detachment and necrosis in
92 the mid-region of the well.

93 Based on simulation results, a hexagonal (divergent-convergent) well performed better than a rectangular well.
94 If the cells are seeded into a rectangular well, they mainly localize in the central zone due to maximum velocity there
95 influenced by boundary layers related to sidewalls (Fig. 2A, red curve). Whereas, velocity profile became more even
96 in a divergent-convergent input due to the reduction cross section area and mitigation of boundary layer effects (Fig.
97 2B, blue curve), resulting in a homogeneous flow velocity and cell distribution across the well at the feeding and
98 seeding times, respectively. We designed 12 wells in each chip for simultaneously RGCs treatment with different
99 compounds per well without any mixing of culture media or cells from one well to another via the gas channels
100 during feeding process. The gas channels necessarily had to be interconnected to provide the same level of pressure
101 and gas conditions to all wells within a chip. A single gas inlet was located for each chip which led to two separate
102 main channels with six branching sub-channels (Fig. 2C).

103 The bottom surface of the wells (layer C) were treated by air plasma to chemical modification and
104 functionalization. This surface treatment increases surface roughness, amount of oxygen atoms, and functional
105 hydrophilic groups (and as a result the number of polar interactions), especially the electron-donor parameters. These
106 modifications enhance cellular adhesion which is fundamental for cell growth, migration, and differentiation.

107 Extracellular microenvironment model on modified PMMA surface

108 ATRA was added to the culture media to differentiate SH-SY5Y neuroblastoma cells into more mature, neuron-
109 like cells. ATRA is a powerful growth inhibitor but promotes normal cellular differentiation. This low cost procedure
110 is easily performed as compared to primary neuronal culture and may generate a homogenous neuronal cell
111 population. The morphology and distribution of neuron-like cells were distinguished by phase-contrast microscopy
112 (Fig. 3A). Untreated neuroblastoma cells possess large and flat cell bodies, however neuron-like cells have branching
113 neuronal networks with smaller and round cell bodies. The neuron-like cells were cultured onto plasma-treated
114 PMMA with different membrane coating to model the extracellular microenvironment in vitro (Fig. 3B).

115 The cellular density was significantly more ordered with PDL/laminin coating as compared to gelatin and
116 collagen membranes, PAN/PANI nanocomposite or non-modified surface (negative control). The SH-SY5Y
117 exhibited better differentiated morphology and more regular pattern of growth on the PDL/laminin membrane.
118 Furthermore, the PDL/laminin membrane induced neurite elongation and branching, while other membranes
119 increased cell aggregation, reminiscent of the aggregation commonly observed in undifferentiated cultures. Due to
120 these reasons, we selected PDL/laminin surface coating for cell culture purposes in the following experiments.

121 ## Characterization of RGCs

122 The steps of RGC isolation by MACS technique are summarized in Fig. 4A. After isolation, flow cytometry
123 showed high purity of RGCs, in which the percentage of RGCs was calculated by determining the ratio of CD90.1-
124 positive cells (Fig. 4B). Isolation of RGCs was initially performed using a mesh filter according to RGC cell size
125 (>40µm) to increase their population from a baseline of 19.8% in the single-cell retinal suspension to 37.4%. In the
126 later stage MACS isolated RGCs according to CD90.1 surface marker in a 'yes or no' decision manner up to 70.4%
127 purification. The RGCs exhibiting CD90.1 were also characterized using immunocytochemistry assay by above-
128 mentioned antibodies and counterstaining with DAPI (Fig. 5).

129 The RGCs were identified by their morphology and immunofluorescence staining characteristics. Dendrites and
130 axons typically appear at opposing poles of the neuronal cell. On non-modified PMMA surface, RGCs tend to form
131 cell clusters with small to media round cell bodies with few extended fine neurites after a 10-day culture. The majority
132 of RGCs on the modified PMMA surface exhibited uniform and round cell bodies, with neurites extending to connect
133 to one other. At day 10, the cells developed a complex dendritic network with numerous neurites and branches (Table
134 1).

Table 1. Morphological changes of primary RGCs at different time intervals on modified and non-modified PMMA surfaces before the pressure experiment. Scale bar= 50 µm.

Time Intervals	Culture on a modified PMMA surface	Culture on non-modified PMMA surface
1 DAY	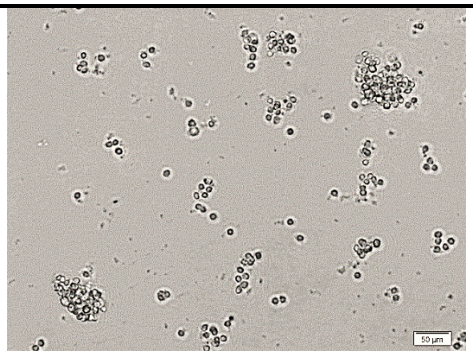	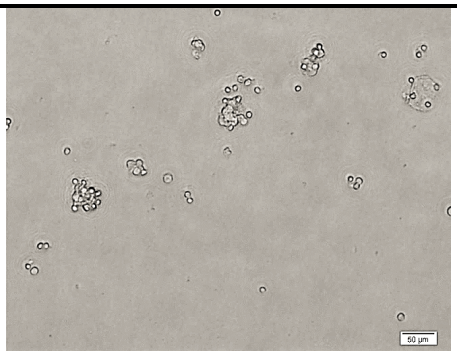
3 DAY	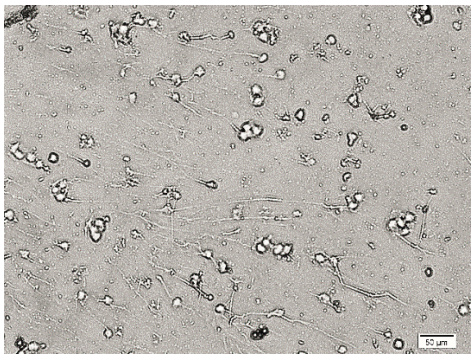	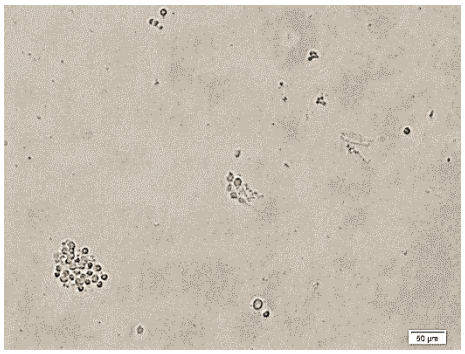
10 DAY	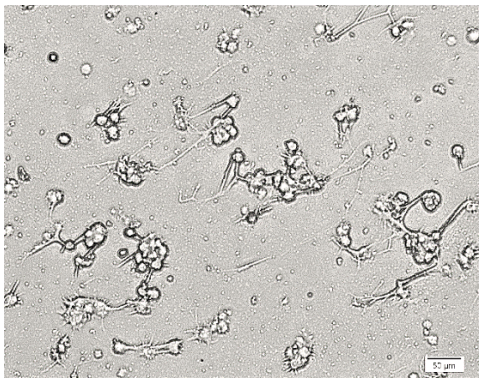	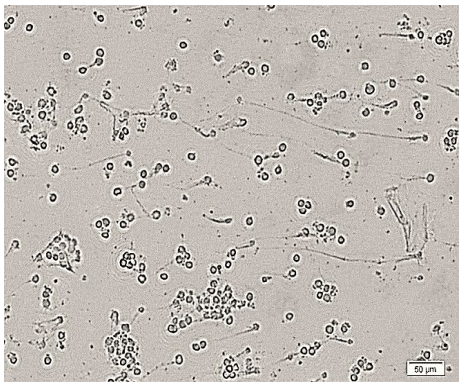
13 DAY	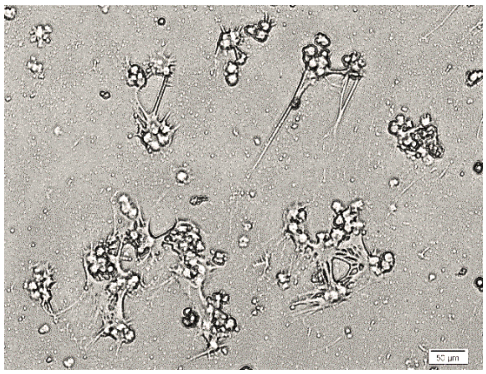	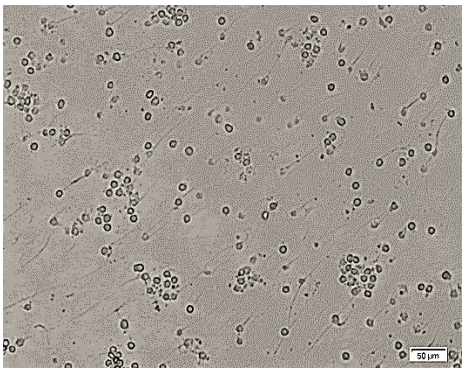

Measurement of Cell Viability

One set of the chips was connected to a gas tank to apply elevated pressure at 33 mmHg, while another chip were exposed to normal pressure at 15 mmHg. As summarized in Figure 6, the EHP system consisted of a compressed 8% CO2/92% air gas tank, which was placed just outside the incubator and adjusted with both regulators for normal and ultra-low delivery pressure. Polyurethane hoses (4/8" ID) were used to feed the gas mixture into the pressure chip through a port at the back of the incubator. A digital pressure gauge (Ashcroft, DG25; 0.5% of 0-15psi span accuracy, ±0.1 mmHg sensitivity; relative to atmospheric pressure) was used to monitor the input pressure value. Pneumatic fittings were placed into the inlet/outlet circuits to provide tight control over gas flow. During loading, the pressure was also monitored by a sensor in the chip and kept at the 33 mm Hg with the accuracy of ±0.1 mmHg (data not shown).

Untreated RGCs decreased in a time-dependent manner when elevated hydrostatic pressure was applied in the chip (Fig. 7A). From 6h of EHP onwards, a significant difference was observed in cell survival as compared to control cells under normal hydrostatic pressure. Cell viability results showed 85, 78, 70, 67 and 61 percent cell survival under normal pressure versus 40, 22, 18, 12 and 10 percent cell survival under high pressure at 6, 12, 24, 36 and 48 hours ($p < 0.0001$), respectively. BDNF-treated RGCs demonstrated better cell survival with or without elevated pressure as compared to untreated cells. BDNF-treated RGCs showed 92, 89, 88, 83 and 80 percent viability under normal pressure compared to 72, 67, 64, 60 and 53 percent under high pressure at 6 ($p = 0.0198$), 12 ($p = 0.0022$), 24 ($p = 0.0004$), 36 ($p < 0.0001$) and 48 ($p < 0.0001$) hours, respectively (Fig. 7B). RNYK provided slightly more stability than BDNF over time. RNYK-treated RGCs showed 94, 93, 89, 87 and 86 percent viability under normal pressure compared to 67, 66, 63, 60 and 58 percent under high pressure at 6, 12, 24, 36 and 48 hours ($p < 0.0001$), respectively (Fig. 7C). BDNF and RNYK treatments induced separately an approximate two-fold decrease in RGC death rates as compared to untreated cells under both normal and elevated pressure condition.

Discussion

Pressure chambers are important tools to study the influence of elevated pressure on individual cell types (Aires et al., 2017). Prior to employing animal models, they allow the assessment of pre-defined experimental conditions and evaluation of specific variables contributing to cell survival. Over the past two decades, various studies have reported significant changes in the behaviour of different cells following the application of hydrostatic pressure (Acevedo et al., 1993; Haberstroh et al., 1999; Hernandez et al., 2000; Kao et al., 2017; Ohashi et al., 2007; Salwen et al., 1998; Schwartz et al., 1999; Sugaya et al., 2003; Thoumine et al., 1995; Tokunaga and Watanabe, 1987; Wax et al., 2000). These changes include increased apoptosis, changes in cell morphology and gene expression. Neuronal cells including PC12 (Agar et al., 2000; Tök et al., 2014) and RGC-5 cell lines (Agar et al., 2006; Ju et al.,

173 2009a; Ju et al., 2007; Lee et al., 2010; Liu et al., 2012), primary cultures of RGC (Sappington et al.,
174 2006; Zhang et al., 2016), optic nerve head astrocytes (Liu and Neufeld, 2001; Liu and Neufeld, 2003;
175 Mandal et al., 2010; Miao et al., 2010; Ricard et al., 2000; Salvador-Silva et al., 2004; Salvador-Silva
176 et al., 2001; Tezel et al., 2001; Yang et al., 2004), Müller cells (Yu et al., 2012a; Yu et al., 2011; Yu et
177 al., 2012b), or microglial cells (Madeira et al., 2015; Sappington and Calkins, 2006; Sappington and
178 Calkins, 2008), and more complex preparations such as organotypic co-cultures of the retinal cells
179 (Obazawa et al., 2004; Osborne et al., 2015; Tezel and Wax, 2000) or eye cup preparations (Ishikawa
180 et al., 2010; Ishikawa et al., 2011; Reigada et al., 2008; Zhang et al., 2007) have been exposed to
181 elevated pressure.

182 In the vast majority of glaucoma patients, IOP levels may vary from 20 to 35 mmHg. Several in
183 vitro glaucoma models have been developed to improve the accuracy and repeatability of experimental
184 conditions in this pressure range. Pressurized chamber is the most commonly used model established
185 by Kosnosky et al. (1995) and modified by Agar at al. (2000) to investigate cellular mechanisms (Agar
186 et al., 2000; Kosnosky et al., 1995). In this system, a mixture of humidified gas is injected through a
187 pressure regulator into a glass macro-chamber with ±1.5 mmHg variation. Studies using this chamber
188 have indicated that exposure of RGC-5 cells to 30, 50, or 100 mmHg for 72, 6, or 2 h, respectively,
189 triggers apoptosis via oxidative stress and mitochondrial dysfunction, similar to the human condition
190 when comparing acute glaucoma (100 mmHg) with chronic glaucoma (30 mmHg) (Agar et al., 2006;
191 Ju et al., 2009a; Ju et al., 2009b; Ju et al., 2007; Liu et al., 2012; Liu et al., 2007; Shang et al., 2014).
192 The second important model is a hydraulic pressurizing chamber introduced by Parkkinen et al. (1993),
193 which compressed the internal gas phase using a hydraulic system (Parkkinen et al., 1993). Tezel and
194 wax (2000) used this device to expose RGCs to 50 mmHg for 72 h and promote neurodegeneration
195 (Tezel and Wax, 2000; Wax et al., 2000).

196 In the present study, we designed a glaucoma-on-a-chip system that provides continuous hydrostatic
197 pressure with ±0.1 mmHg variation under a temperature-controlled environment. Our system was
198 custom-made in agree with the pressurized chamber approach, thus, several conditions and confounding
199 factors were carefully simulated, validated or controlled beforehand. They consisted of fluid velocity
200 fields, alterations in gas composition, temperature and osmolarity to design a more stable and adjustable
201 experiment compared to prior in vitro studies. Our results indicated that glaucoma-on-a-chip can
202 simulate glaucomatous conditions only when provided with a suitable microenvironment for cell-to-
203 cell communication of RGCs. Accordingly, the PMMA surface was modified by air plasma and a thin
204 layer of PDL/laminin to form a continuous surface of mechanical properties and uniform chemistry
205 leading to a homogenous cell distribution. Furthermore, the evaluation of cellular mechanisms requires
206 isolation and culture of primary RGCs. Early postnatal tissues were used to optimize RGC viability in
207 primary cell cultures due to the limited yield and the typically post-mitotic feature of these neurons in

208 the next state. The use of RGCs in cultures on chips allowed examining a direct in vitro situation in
209 which retinal cells maintain their microarchitecture.

210 Most reports investigating the degenerative effect of chronic IOP elevation have used pressures
211 ranging from 30 mmHg (for 72 h) to 100 mmHg (for 2 h), as already described. In the present study,
212 we exposed RGCs to 33 mmHg (elevated hydrostatic pressure, EHP) or 15 mmHg (normal pressure)
213 for 6, 12, 24, 36 and 48 hours, with and without adding neuroprotective agents. Accordingly, cell
214 survival of primary rat RGCs was evaluated under four different experimental conditions simulating
215 the high pressure glaucoma (untreated RGCs under EHP), normal-tension glaucoma (BDNF deprived
216 RGCs under normal pressure), neuroprotective-treated glaucoma (BDNF/RNYK treated RGCs under
217 EHP), and normal conditions (BDNF-treated RGCs under normal pressure). Our results demonstrated
218 that BDNF can maintain neuronal viability despite high pressure. According to cell survival patterns
219 and rates, the neuroprotective influence of BDNF seems to cancel the detrimental effect of elevated
220 pressure. This suggests that the negative impact of neurotrophin deprivation can be compared to the
221 insult of high pressure. This may be equivalent to the observation that failure of axonal transport of
222 neurotrophins in glaucoma triggers RGC degeneration and that retinal cells essentially require
223 neurotrophic input from target neurons in the brain.(Baltmr et al., 2010; Nickells, 2012)

224 This previously confirmed that RNYK can mimic BDNF activities in vitro at an optimum
225 concentration of 5 ng ml^{-1}. RNYK prevented neuronal degeneration of ATRA-treated SH-SY5Y with
226 equal efficacy to or even better than BDNF at 50 ng ml^{-1} (Nafian et al., 2018). In the current study,
227 RNYK indicated a neuroprotective effect comparable to BDNF on primary RGCs under both normal
228 and elevated pressures. In light of the findings obtained, the identified peptidomimetic compound is
229 significant as a promising neuroprotective agent for glaucoma treatment. Also, small size of RNYK
230 might be an advantage for drug design and synthesis in future. It is clear that in vitro models may never
231 substitute animal studies, but they are important tools in preclinical studies. Glaucoma-on-a-chip offers
232 the advantages of allowing controlled experimental conditions, preliminary targeting of a specific cell
233 type or pathway involved in glaucomatous damage. More studies are needed to develop models to study
234 RGC neurodegeneration and neuroprotection by putative agents such as neurotrophins, peptides, and
235 other small molecules prior to assessment in animal models.

236 Material and methods

237 Design of a three-layered chip

238 In order to induce a high pressure environment to simulate glaucomatous conditions, several three-
239 layered EHP models were designed. A number of morphological parameters were considered including
240 number and location of feeding ports in the top layer (layer A), the shape of micro-channels and wells
241 in the middle layer (layer B), and surface modification for the bottom layer (layer C) of the chip.
242 AutoCAD 2014 was used to design the layers. Some physical parameters including gas concentrations

and fluid velocity profile for media at seeding/feeding time were simulated by Comsol Multiphysics 5.2a software employing finite element methods. Two-dimensional incompressible Navier-Stokes equations were used along with the continuity equation to determine the liquid velocity profile of culture media throughout the fluid dynamic field at the seeding and feeding time

$$\nabla \cdot \boldsymbol{u} = 0 \quad (1)$$

$$\rho \boldsymbol{u} \cdot \nabla \boldsymbol{u} = -\nabla p + \mu \nabla^2 \boldsymbol{u} \quad (2)$$

Where **u** is the velocity vector, p is the pressure of injection, ρ is the density of media, and μ is the dynamic viscosity. The no-slip boundary condition was assumed at the walls. Constant velocity was specified at the inlet. The outlet was assumed to be at atmospheric pressure.

After the flow reached a steady-state condition, gas was assumed to be transported only by diffusion so that gas distribution was estimated using Fick's law (FL). Gas was released at the inlet at a specific concentration (C_0), which was monitored after a certain sampling time period. The transient two-dimensional mass transport equation is as follows:

$$\frac{\partial C}{\partial t} + \mathbf{u} \cdot \nabla C = D \nabla^2 C \quad (3)$$

Where C is the gas concentration in the bulk, and D is the diffusion coefficient.

A novel low-cost fabrication method was established to produce the three-layered chip entirely from poly-methyl methacrylate (PMMA, Cho Chen, Company, city, country). PMMA is the most common member of the acrylic family. The optical clarity and ability to resist environmental stress make PMMA ideal for replacing glass in light transmission applications (Henkel, 2011). PMMA biocompatibility has been established through years in medicine and ophthalmology (Frazer et al., 2005).

Fabrication and testing of the three-layered chip

A laser system (fiber laser, PNC laser Co. Ltd, Tehran, Iran) was used to cut polymerized PMMA sheets of about 10mm thickness for layer B and 2mm for layers A and C. The laser processing system was equipped with a programming system (NC system), an automatic programming combining computer and CAD technology. When using the laser for fabricating channels and wells on PMMA sheet, the laser power and scanning speed were considered as main factors. Several tests were performed to explore the correct correlation between laser power and scanning speed. A 25W laser power and a 300mm/s laser scanning speed were selected to produce main channels and sub-channels on layer B. In addition, 20W and 45W laser power were applied to cut PMMA sheets 10 mm and 2 mm in thickness respectively, at 100 mm/s laser scanning speed to make the wells and ports in layers A and B.

274 A thermal-solvent method was used to attach the three layers of any single chip. This method is
275 based on dissolving PMMA in a thin layer of a solvent (isopropyl alcohol) between two PMMA
276 substrates at 75 °C for 10 min (Bamshad et al., 2016). Adhesion of PMMA substrates involved the
277 following steps. First, the layers cut by the laser were rinsed in deionized water for 5 minutes to remove
278 tiny debris and dried at 40 °C for 10 minutes in an oven. Next the solvent was added between layers B
279 and C which were aligned and fixed using paper clamps to avoid entrapment of air bubbles between the
280 binding surfaces. The attached sheets were heated and finally treated with air plasma. Radiofrequency
281 discharged plasma was generated by a dinner plasma generator from Dinner CO. at 13.6 MHZ
282 frequency and 20W power for 10 min. The base pressure of the plasma reactor was increased to 0.35
283 mmHg after gas feeding. After attaching layers B and C, layer A was attached using the same method
284 described above to complete the three-layered chip.

285 Extracellular microenvironment model on modified PMMA surface

286 SH-SY5Y cell line which is the third sequential sub-clone of the SKN-SH human neuroblastoma
287 cell line was purchased from the Pasteur Institute (Tehran, Iran). These cells phenotypically change
288 from neuronal type (N) to surface adherent type (S) by all-trans-retinoic acid (ATRA) treatment
289 (Kovalevich and Langford, 2013). The cells were seeded at an initial density of 10^4 cells per cm^2 in the
290 wells of the chip, which were pre-coated with one of the following membranes: collagen (0.05 mg ml^{-}
291 ^{1}), ploy-D-lysine (PDL)/laminin (0.01 mg ml^{-1}/0.05 mg ml^{-1}), gelatine (1 mg ml^{-1}), and a composite
292 nanofiber of polyacrylonitrile (PAN) and polyaniline (PANI), named PAN/PANI. When the cells were
293 approximately 75% confluent, ATRA (Sigma-Aldrich, Vienna, Austria) treatment was performed at a
294 final concentration of 10 µM in Dulbecco's modified Eagle's medium (DMEM) (Gibco-BRL *Life*
295 *Technologies*, *Grand Island*, NY) supplemented with 2 mM L-glutamine, penicillin (20 U ml^{-1}),
296 streptomycin (20 mg ml^{-1}), and 15% (by volume) Fetal Bovine Serum *(FBS) (Gibco-BRL Life*
297 *Technologies*) and incubated for 5 days. Cell morphology, density, and distribution were compared
298 among different coating materials.

299 Purification of RGCs and primary culture in the chip wells

300 Forty-eight hours before the experiment, chip surface was modified using plasma jet and exposed
301 to UV light for 1h to assess successful sterilization. Then, 500 µl of PDL solution (Sigma-Aldrich), 10
302 µg ml^{-1} was added to each well for 1h. The wells were washed three times with sterile water and
303 completely dried. The day before the experiment, 500 µl of laminin solution (5 µg ml^{-1}, Sigma-Aldrich)
304 prepared in Neurobasal medium was added to each well and incubated overnight at 37°C (8% CO2).
305 The laminin/Neurobasal solution was replaced with 500 µl of "retinal ganglion cell media" which was
306 prepared as follows: Neurobasal medium (Gibco-BRL Life Technologies) with 1% bovine serum
307 albumin (BSA, Sigma-Aldrich), sodium selenite (6.7 ng ml^{-1}, Sigma-Aldrich), Insulin-Transferrin-
308 Selenium (ITS-G) (100X) (Thermo Fisher Scientific, Grand Island, New York, USA), progesterone (20

309 nM; Merck Millipore), B27 Supplement (50X) (Thermo Fisher Scientific), sodium pyruvate (1 mM;
310 Merck Millipore), L-Glutamine (100x) (2 mM; Gibco-BRL Life Technologies), penicillin (20 U ml^{-1}),
311 and streptomycin (20 mg ml^{-1}).

312 In accordance with the regulations of association for research in vision and ophthalmology (ARVO)
313 for animal studies, ten postnatal day's five to seven Wistar rats (Razi Institute, Karaj, Iran) were
314 sacrificed by decapitation and then enucleated. The cornea, lens, and vitreous humor were removed and
315 the retina was gently lifted away using a small spatula. The retinas were stored at room temperature in
316 4.5 ml Hank's balanced salt solution, Ca2+ and Mg2+ free (HBSS-CMF, Sigma-Aldrich), pH 7.4. Then,
317 0.5 ml of trypsin (2.5%, Gibco-BRL *Life Technologies*) was added to the tube containing five retinas
318 and incubated in a water bath at 37˚C for 15 min where the tube was gently swirled every 5 min. The
319 HBSS/trypsin solution was replaced by 5 ml of HBSS (containing 50 µl of DNase I 0.4%) and incubated
320 at 37˚C for 5 min. The retina was converted into a cell suspension by triturating and homogenizing the
321 solution without introducing bubbles. The cells were centrifuged at 300g for 5 min and re-suspended in
322 1ml HBSS containing 0.5 mg ml^{-1} BSA. The cell suspension was filtered through a mesh filter (pore
323 size 40 µm, BD Falcon, Franklin Lakes, NJ) to yield a single cell suspension.

324 For magnetic assisted cell sorting (MACS), a concentration of 10^7 retinal cells per 90 µl of
325 DBPS/BSA buffer (Dulbecco's PBS containing 0.5 mg ml^{-1} BSA) was incubated with 10 µl of the RGC-
326 specific marker CD90.1 microbeads (Miltenyi Biotec, GmbH, and Bergisch Gladbach, Germany) at
327 room temperature for 30 min and then washed with 5 ml of DPBS/BSA buffer. The cell suspension was
328 passed through an LS column to hold the micro bead-labelled cells (RGCs) in the magnetic field of a
329 MidiMACS system (Miltenyi Biotec). The adherent RGCs were rinsed with 3 ml of DPBS/BSA buffer
330 to deplete endothelial cells and microglia. The column was removed from the separator and held over
331 a new 15-ml tube. The adhered cells were flushed out by firmly pushing the plunger into the column
332 and counted.

333 Flow cytometry and immunocytochemistry of RGCs

334 In different isolation steps, cells were stained with mouse anti-CD90.1 antibody (Millipore,
335 Bedford, MA) and goat anti-mouse IgG antibody FITC conjugated (Santa Cruz Biotechnology, Inc.,
336 Dallas, USA) as primary and secondary antibodies, respectively. The anti-CD90.1 antibody was added
337 to the cell suspension at a concentration of 0.1 µg per 100 µl for 10^6 cells and incubated at 4˚C for 20
338 min. The cells were washed three times with PBS buffer and then 100 µl anti-mouse IgG antibody FITC
339 conjugated was added (1:100 dilution) and incubated at room temperature for 30 min in the dark. After
340 3-times washing, the fluorescence emission intensity was measured using a flow cytometer. FlowJo
341 (Tree Star, Inc., Ashland, OR) was used to exclude dead cells from the analysis based on scatter signals.
342 The number of cells exhibiting CD90.1 were manually counted, and the RGC percentage was calculated
343 by determining the rate of CD90.1-positive cells relative to other ones.

Purified RGCs were cultured on a chip pre-coated with PDL/laminin at 37˚C and 8% CO2. After a 3-day culture, RGCs were fixed with cold methanol (-10˚C) for 10 min, dried, and then blocked with 300µl of PBS containing 1% BSA for 20 min at room temperature. The cells were incubated with 10 µl mouse anti-CD90.1 antibody (1:100 dilution) as a primary antibody overnight at 4 °C. RGCs were exposed to goat anti-mouse IgG antibody FITC conjugated as a corresponding fluorescent secondary antibody (1:100 dilution) at room temperature for 1 h in the dark. Nuclei were counterstained with 4',6-diamidino-2-phenylindole (DAPI, Thermo Fisher Scientific, Pennsylvania, USA) as a colouring reagent. To determine the expression of specific marker on the RGC surface (CD90.1-positive cells), several random fields were imaged under a fluorescence microscope.

Measurement of Cell Viability

RGCs were seeded at an initial density of 10^4 cells per cm2 in two sets of 12-well chips prior to the pressure experiment. RGCs were exposed to high hydrostatic pressures in a time-dependent manner for 6, 12, 24, 36 and 48 hours. BDNF (50 ng ml^{-1}; Thermo Fisher Scientific, Waltham, USA) and RNYK peptide (5 ng ml^{-1}) were separately applied to RGCs in one chip under normal and the other elevated hydrostatic pressure. RGCs in control groups did not receive BDNF/RNYK in the same experiments. The chip pressure was checked periodically by tonometer for fluctuations to hold the pressure level constant in each test. Cell viability was measured using 3-(4, 5-dimethylthiazol-2-yl)-2, 5-diphenyltetrazolium bromide (MTT, Sigma-Aldrich) assay for each well in the six groups. MTT solution was added to the media at a final concentration of 0.5 mg ml^{-1} and aspirated from the wells after 4 h. The residual crystals (formazan) were dissolved in dimethyl sulfoxide (DMSO, Sigma-Aldrich) and the absorbance was measured at near 570 nm. These experiments were repeated for at least three times to check the reproducibility of biologic effects. All measured variables were described as mean ±SD.

Statistical Analysis

Cell viability in BDNF/RNYK treatment groups was compared to that of untreated controls under normal and elevated pressure. The GraphPad Prism 7.0 statistical software was employed (San Diego, USA). Significance was determined at $p < 0.05$ level using two-way ANOVA with Holm-Sidak's multiple comparison test.

Conflicts of interest

The authors declare that no conflict of interest exists.

Acknowledgements

We are thankful to Dr. S Gharavi (Alzahra University, Tehran, Iran) and Dr. N K Tafreshi (Moffitt Cancer Center and Research Institute, Florida, USA) for technical support.

References

Acevedo, A. D., Bowser, S. S., Gerritsen, M. E. and Bizios, R. (1993). Morphological and proliferative responses of endothelial cells to hydrostatic pressure: role of fibroblast growth factor. *Journal of Cellular Physiology*. **157**, 603-614.

Agar, A., Li, S., Agarwal, N., Coroneo, M. T. and Hill, M. A. (2006). Retinal ganglion cell line apoptosis induced by hydrostatic pressure. *Brain Research*. **1086**, 191-200.

Agar, A., Yip, S. S., Hill, M. A. and Coroneo, M. T. (2000). Pressure related apoptosis in neuronal cell lines. *Journal of Neuroscience Research*. **60**, 495-503.

Aires, I., Ambrósio, A. and Santiago, A. (2017). Modeling Human Glaucoma: Lessons from the in vitro Models. *Ophthalmic Research*. **57**, 77-86.

Balijepalli, A. and Sivaramakrishan, V. (2017). Organs-on-chips: research and commercial perspectives. *Drug discovery today*. **22**, 397-403.

Baltmr, A., Duggan, J., Nizari, S., Salt, T. E. and Cordeiro, M. F. (2010). Neuroprotection in glaucoma–is there a future role? *Experimental Eye Research*. **91**, 554-566.

Bamshad, A., Nikfarjam, A. and Khaleghi, H. (2016). A new simple and fast thermally-solvent assisted method to bond PMMA–PMMA in micro-fluidics devices. *Journal of Micromechanics and Microengineering*. **26**, 1-12.

Dai, M., Zhang, Q., Zheng, Z. and Wang, J. (2018). Retinal ganglion cell-conditioned medium and surrounding pressure alters gene expression and differentiation of rat retinal progenitor cells. *Molecular Medicine Reports*. **17**, 7177-7183.

El-Ali, J., Sorger, P. K. and Jensen, K. F. (2006). Cells on chips. *Nature*. **442**, 403-411.

Esch, E. W., Bahinski, A. and Huh, D. (2015). Organs-on-chips at the frontiers of drug discovery. *Nature reviews Drug discovery*. **14**, 248–260.

Fedorchak, M. V., Conner, I. P., Medina, C. A., Wingard, J. B., Schuman, J. S. and Little, S. R. (2014). 28-day intraocular pressure reduction with a single dose of brimonidine tartrate-loaded microspheres. *Experimental Eye Research*. **125**, 210-216.

Frazer, R. Q., Byron, R. T., Osborne, P. B. and West, K. P. (2005). PMMA: an essential material in medicine and dentistry. *Journal of Long-Term Effects of Medical Implants*. **15**, 629-639.

Gaasterland, D. and Kupfer, C. (1974). Experimental glaucoma in the rhesus monkey. *Investigative Ophthalmology and Visual Science*. **13**, 455-457.

Haberstroh, K. M., Kaefer, M., Retik, A. B., Freeman, M. R. and Bizios, R. (1999). The effects of sustained hydrostatic pressure on select bladder smooth muscle cell functions. *The Journal of urology*. **162**, 2114-2118.

Henkel, C. (2011). Design Guide for Bonding Plastics. *Henkel Corporation*. **6**, 1-100.

Hernandez, M. R., Pena, J. D., Selvidge, J. A., Salvador-Silva, M. and Yang, P. (2000). Hydrostatic pressure stimulates synthesis of elastin in cultured optic nerve head astrocytes. *Glia*. **32**, 122-136.

Ingber, D. E. (2016). Reverse engineering human pathophysiology with organs-on-chips. *Cell*. **164**, 1105-1109.

Ishikawa, M., Yoshitomi, T., Covey, D. F., Zorumski, C. F. and Izumi, Y. (2016). TSPO activation modulates the effects of high pressure in a rat ex vivo glaucoma model. *Neuropharmacology*. **111**, 142-159.

Ishikawa, M., Yoshitomi, T., Covey, D. F., Zorumski, C. F. and Izumi, Y. (2018). Additive neuroprotective effects of 24 (S)-hydroxycholesterol and allopregnanolone in an ex vivo rat glaucoma model. *Scientific Reports*. **8**, 1-15.

Ishikawa, M., Yoshitomi, T., Zorumski, C. F. and Izumi, Y. (2010). Effects of acutely elevated hydrostatic pressure in a rat ex vivo retinal preparation. *Investigative Ophthalmology and Visual Science*. **51**, 6414-6423.

Ishikawa, M., Yoshitomi, T., Zorumski, C. F. and Izumi, Y. (2011). Downregulation of glutamine synthetase via GLAST suppression induces retinal axonal swelling in a rat ex vivo hydrostatic pressure model. *Investigative Ophthalmology and Visual Science*. **52**, 6604-6616.

Ishikawa, M., Yoshitomi, T., Zorumski, C. F. and Izumi, Y. (2014). Neurosteroids are endogenous neuroprotectants in an ex vivo glaucoma model. *Investigative Ophthalmology and Visual Science*. **55**, 8531-8541.

Ishikawa, M., Yoshitomi, T., Zorumski, C. F. and Izumi, Y. (2015). Experimentally induced mammalian models of glaucoma. *BioMed research international*. **2015**, 1-11.

Johnson, T. V. and Tomarev, S. I. (2010). Rodent models of glaucoma. *Brain Research Bulletin*. **81**, 349-358.

Ju, W.-K., Kim, K.-Y., Lindsey, J. D., Angert, M., Patel, A., Scott, R. T., Liu, Q., Crowston, J. G., Ellisman, M. H. and Perkins, G. A. (2009a). Elevated hydrostatic pressure triggers release of OPA1 and cytochrome C, and induces apoptotic cell death in differentiated RGC-5 cells. *Molecular Vision*. **15**, 120-134.

Ju, W.-K., Liu, Q., Kim, K.-Y., Crowston, J. G., Lindsey, J. D., Agarwal, N., Ellisman, M. H., Perkins, G. A. and Weinreb, R. N. (2007). Elevated hydrostatic pressure triggers mitochondrial fission and decreases cellular ATP in differentiated RGC-5 cells. *Investigative Ophthalmology and Visual Science*. **48**, 2145-2151.

Kalvin, N., Hamasaki, D. and Gass, J. (1966). Experimental glaucoma in monkeys: I. Relationship between intraocular pressure and cupping of the optic disc and cavernous atrophy of the optic nerve. *Archives of Ophthalmology*. **76**, 82-93.

Kao, Y., Jheng, J., Pan, H., Liao, W., Lee, C. and Kuo, P. (2017). Elevated hydrostatic pressure enhances the motility and enlarges the size of the lung cancer cells through aquaporin upregulation mediated by caveolin-1 and ERK1/2 signaling. *Oncogene*. **36**, 863-874.

Kosnosky, W., Tripathi, B. and Tripathi, R. (1995). An in-vitro system for studying pressure effects on growth, morphology, and biochemical aspects of trabecular meshwork cells. In *Investigative Ophthalmology and Visual Science*. **36**, S731-S731.

Kovalevich, J. and Langford, D. (2013). Considerations for the use of SH-SY5Y neuroblastoma cells in neurobiology. In *Neuronal Cell Culture*, vol. 1078, pp. 9-21: Springer.

Lee, J. K., Lu, S. and Madhukar, A. (2010). Real-time dynamics of Ca2+, caspase-3/7, and morphological changes in retinal ganglion cell apoptosis under elevated pressure. *PloS One*. **5**, e13437.

Lei, Y., Rajabi, S., Pedrigi, R. M., Overby, D. R., Read, A. T. and Ethier, C. R. (2011). In vitro models for glaucoma research: effects of hydrostatic pressure. *Investigative Ophthalmology and Visual Science*. **52**, 6329-6339.

Levin, L. A., Nilsson, S. F., Ver Hoeve, J., Wu, S., Kaufman, P. L. and Alm, A. (2011). Adler's Physiology of the Eye E-Book: Elsevier Health Sciences.

Liu, B., Ma, X., Guo, D., Guo, Y., Chen, N. and Bi, H. (2012). Neuroprotective effect of alpha-lipoic acid on hydrostatic pressure-induced damage of retinal ganglion cells in vitro. *Neuroscience Letters*. **526**, 24-28.

Liu, B. and Neufeld, A. H. (2001). Nitric oxide synthase-2 in human optic nerve head astrocytes induced by elevated pressure in vitro. *Archives of Ophthalmology*. **119**, 240-245.

Liu, B. and Neufeld, A. H. (2003). Activation of epidermal growth factor receptor signals induction of nitric oxide synthase-2 in human optic nerve head astrocytes in glaucomatous optic neuropathy. *Neurobiology of Disease*. **13**, 109-123.

Liu, Q., Ju, W.-K., Crowston, J. G., Xie, F., Perry, G., Smith, M. A., Lindsey, J. D. and Weinreb, R. N. (2007). Oxidative stress is an early event in hydrostatic pressure–induced retinal ganglion cell damage. *Investigative Ophthalmology and Visual Science*. **48**, 4580-4589.

Madeira, M. H., Elvas, F., Boia, R., Gonçalves, F. Q., Cunha, R. A., Ambrósio, A. F. and Santiago, A. R. (2015). Adenosine A 2A R blockade prevents neuroinflammation-induced death of retinal ganglion cells caused by elevated pressure. *Journal of Neuroinflammation*. **12**, 115-128.

Mandal, A., Shahidullah, M. and Delamere, N. A. (2010). Hydrostatic pressure–induced release of stored calcium in cultured rat optic nerve head astrocytes. *Investigative Ophthalmology and Visual Science*. **51**, 3129-3138.

Maurya, N., Agarwal, N. R. and Ghosh, I. (2016). Low-dose rotenone exposure induces early senescence leading to late apoptotic signaling cascade in human trabecular meshwork (HTM) cell line: An in vitro glaucoma model. *Cell Biology International*. **40**, 107-120.

Miao, H., Crabb, A. W., Hernandez, M. R. and Lukas, T. J. (2010). Modulation of factors affecting optic nerve head astrocyte migration. *Investigative Ophthalmology and Visual Science*. **51**, 4096-4103.

Morrison, J. C., Moore, C., Deppmeier, L. M., Gold, B. G., Meshul, C. K. and Johnson, E. C. (1997). A rat model of chronic pressure-induced optic nerve damage. *Experimental Eye Research*. **64**, 85-96.

Nafian, F., Rasaee, M., Yazdani, S., Daftarian, N., Soheili, Z. and Kamali Doust Azad, B. (2018). Peptide selected by phage display increases survival of SH-SY5Y neurons comparable to brain-derived neurotrophic factor. *Journal of Cellular Biochemistry*. **120**, 1-11.

Nickells, R. W. (2012). The cell and molecular biology of glaucoma: mechanisms of retinal ganglion cell death. *Investigative Ophthalmology and Visual Science*. **53**, 2476-2481.

Obazawa, M., Mashima, Y., Sanuki, N., Noda, S., Kudoh, J., Shimizu, N., Oguchi, Y., Tanaka, Y. and Iwata, T. (2004). Analysis of porcine optineurin and myocilin expression in trabecular meshwork cells and astrocytes from optic nerve head. *Investigative Ophthalmology and Visual Science*. **45**, 2652-2659.

Ohashi, T., Sugaya, Y., Sakamoto, N. and Sato, M. (2007). Hydrostatic pressure influences morphology and expression of VE-cadherin of vascular endothelial cells. *Journal of Biomechanics*. **40**, 2399-2405.

Osborne, A., Aldarwesh, A., Rhodes, J. D., Broadway, D. C., Everitt, C. and Sanderson, J. (2015). Hydrostatic pressure does not cause detectable changes in survival of human retinal ganglion cells. *PloS One*. **10**, 1-14.

Parkkinen, J., Ikonen, J., Lammi, M., Laakkonen, J., Tammi, M. and Helminen, H. (1993). Effects of cyclic hydrostatic pressure on proteoglycan synthesis in cultured chondrocytes and articular cartilage explants. *Archives of Biochemistry and Biophysics*. **300**, 458-465.

Quigley, H. A. and Addicks, E. M. (1980). Chronic experimental glaucoma in primates. I. Production of elevated intraocular pressure by anterior chamber injection of autologous ghost red blood cells. *Investigative Ophthalmology and Visual Science*. **19**, 126-136.

Reigada, D., Lu, W., Zhang, M. and Mitchell, C. H. (2008). Elevated pressure triggers a physiological release of ATP from the retina: possible role for pannexin hemichannels. *Neuroscience*. **157**, 396-404.

Ricard, C. S., Kobayashi, S., Pena, J. D., Salvador-Silva, M., Agapova, O. and Hernandez, M. R. (2000). Selective expression of neural cell adhesion molecule (NCAM)-180 in optic nerve head astrocytes exposed to elevated hydrostatic pressure in vitro. *Molecular brain research*. **81**, 62-79.

Rieck, J. (2013). The pathogenesis of glaucoma in the interplay with the immune system. *Investigative Ophthalmology and Visual Science*. **54**, 2393-2409.

Rudzinski, M. and Saragovi, H. U. (2005). Glaucoma: validated and facile in vivo experimental models of a chronic neurodegenerative disease for drug development. *Current Medicinal Chemistry-Central Nervous System Agents*. **5**, 43-49.

Salvador-Silva, M., Aoi, S., Parker, A., Yang, P., Pecen, P. and Hernandez, M. R. (2004). Responses and signaling pathways in human optic nerve head astrocytes exposed to hydrostatic pressure in vitro. *Glia*. **45**, 364-377.

Salvador-Silva, M., Ricard, C. S., Agapova, O. A., Yang, P. and Hernandez, M. R. (2001). Expression of small heat shock proteins and intermediate filaments in the human optic nerve head astrocytes exposed to elevated hydrostatic pressure in vitro. *Journal of Neuroscience Research*. **66**, 59-73.

Salwen, S., Szarowski, D., Turner, J. and Bizios, R. (1998). Three-dimensional changes of the cytoskeleton of vascular endothelial cells exposed to sustained hydrostatic pressure. *Medical and Biological Engineering and Computing*. **36**, 520-527.

Sappington, R. M. and Calkins, D. J. (2006). Pressure-induced regulation of IL-6 in retinal glial cells: involvement of the ubiquitin/proteasome pathway and NFκB. *Investigative Ophthalmology and Visual Science*. **47**, 3860-3869.

Sappington, R. M. and Calkins, D. J. (2008). Contribution of TRPV1 to microglia-derived IL-6 and NFκB translocation with elevated hydrostatic pressure. *Investigative Ophthalmology and Visual Science*. **49**, 3004-3017.

Sappington, R. M., Chan, M. and Calkins, D. J. (2006). Interleukin-6 protects retinal ganglion cells from pressure-induced death. *Investigative Ophthalmology and Visual Science*. **47**, 2932-2942.

Schwartz, E. A., Bizios, R., Medow, M. S. and Gerritsen, M. E. (1999). Exposure of human vascular endothelial cells to sustained hydrostatic pressure stimulates proliferation: involvement of the αv integrins. *Circulation Research*. **84**, 315-322.

Shang, L., Huang, J.-F., Ding, W., Chen, S., Xue, L.-X., Ma, R.-F. and Xiong, K. (2014). Calpain: a molecule to induce AIF-mediated necroptosis in RGC-5 following elevated hydrostatic pressure. *BMC Neuroscience*. **15**, 63.

Shareef, S., Garcia-Valenzuela, E., Salierno, A., Walsh, J. and Sharma, S. (1995). Chronic ocular hypertension following episcleral venous occlusion in rats. *Experimental Eye Research*. **61**, 379-382.

Sugaya, Y., Sakamoto, N., Ohashi, T. and Sato, M. (2003). Elongation and random orientation of bovine endothelial cells in response to hydrostatic pressure: comparison with response to shear stress. *JSME International Journal Series C Mechanical Systems, Machine Elements and Manufacturing*. **46**, 1248-1255.

Tezel, G., Hernandez, M. R. and Wax, M. B. (2001). In vitro evaluation of reactive astrocyte migration, a component of tissue remodeling in glaucomatous optic nerve head. *Glia*. **34**, 178-189.

Tezel, G. and Wax, M. B. (2000). Increased production of tumor necrosis factor-α by glial cells exposed to simulated ischemia or elevated hydrostatic pressure induces apoptosis in cocultured retinal ganglion cells. *Journal of Neuroscience*. **20**, 8693-8700.

Tham, Y.-C., Li, X., Wong, T. Y., Quigley, H. A., Aung, T. and Cheng, C.-Y. (2014). Global prevalence of glaucoma and projections of glaucoma burden through 2040: a systematic review and meta-analysis. *Ophthalmology*. **121**, 2081-2090.

Thoumine, O., Nerem, R. M. and Girard, F. R. (1995). Oscillatory shear stress and hydrostatic pressure modulate cell-matrix attachment proteins in cultured endothelial cells. *In Vitro Cellular & Developmental Biology-Animal*. **31**, 45-54.

Tök, L., Nazıroğlu, M., Uğuz, A. C. and Tök, Ö. (2014). Elevated hydrostatic pressures induce apoptosis and oxidative stress through mitochondrial membrane depolarization in PC12 neuronal cells: A cell culture model of glaucoma. *Journal of Receptors and Signal Transduction*. **34**, 410-416.

Tokunaga, O. and Watanabe, T. (1987). Properties of endothelial cell and smooth muscle cell cultured in ambient pressure. *In Vitro Cellular and Developmental Biology*. **23**, 528-534.

Vecino, E. and Sharma, S. C. (2011). Glaucoma animal models. In *Glaucoma-Basic and Clinical Concepts*. **15**, 320-334.

Wax, M. B., Tezel, G., Kobayashi, S. and Hernandez, M. R. (2000). Responses of different cell lines from ocular tissues to elevated hydrostatic pressure. *British Journal of Ophthalmology*. **84**, 423-428.

Yang, P., Agapova, O., Parker, A., Shannon, W., Pecen, P., Duncan, J., Salvador-Silva, M. and Hernandez, M. R. (2004). DNA microarray analysis of gene expression in human optic nerve head astrocytes in response to hydrostatic pressure. *Physiological genomics*. **17**, 157-169.

Yu, J., Chen, C., Wang, J., Cheng, Y., Wu, Q., Zhong, Y. and Shen, X. (2012a). In vitro effect of adenosine on the mRNA expression of Kir 2.1 and Kir 4.1 channels in rat retinal Müller cells at elevated hydrostatic pressure. *Experimental and Therapeutic Medicine*. **3**, 617-620.

Yu, J., Zhong, Y., Cheng, Y., Shen, X., Wang, J. and Wei, Y. (2011). Effect of high hydrostatic pressure on the expression of glutamine synthetase in rat retinal Müller cells cultured in vitro. *Experimental and Therapeutic Medicine*. **2**, 513-516.

Yu, J., Zhong, Y., Shen, X., Cheng, Y., Qi, J. and Wang, J. (2012b). In vitro effect of adenosine A2A receptor antagonist SCH 442416 on the expression of glutamine synthetase and glutamate aspartate transporter in rat retinal Müller cells at elevated hydrostatic pressure. *Oncology Reports*. **27**, 748-752.

Zhang, S.-H., Gao, F.-J., Sun, Z.-M., Xu, P., Chen, J.-Y., Sun, X.-H. and Wu, J.-H. (2016). High pressure-induced mtDNA alterations in retinal ganglion cells and subsequent apoptosis. *Frontiers in Cellular Neuroscience*. **10**, 254-264.

Zhang, X., Li, A., Ge, J., Reigada, D., Laties, A. M. and Mitchell, C. H. (2007). Acute increase of intraocular pressure releases ATP into the anterior chamber. *Experimental Eye Research*. **85**, 637-643.

571 Figure 1. Schematic of a designed chip in AutoCAD software. (A) Three-dimensional design of layers
572 A (1), B (2), and C (3) containing 12 wells (4), feeding ports (5), and microchannels (6), 2 main
573 channels (7) and 1 single gas inlet (8). Layer A consisted of one feeding port per well and one main gas
574 inlet. Layer B involved 12 hexagonal wells and microchannels. Layer C provided a surface area for cell
575 cultures. Layers were fabricated (B) and assembled (C) to establish a complete chip.

576 Figure 2. Estimated velocity profiles and gas concentration by Comsol Multiphysics software. (A) An
577 entrance region was observed where the upstream flow entered the rectangular well. The boundary layer
578 increased downstream, delayed the axial flow at the wall and accelerated the core flow in the center by
579 maintaining the same flow rate. (B) The velocity profile became more even across the hexagonal well
580 by straitening the walls at the entrance region and reducing the boundary layers at downstream (C) Gas
581 concentration slightly changed throughout the main channels, sub-channels, and wells.

582 Figure 3. Phase contrast images of SH-SY5Y cells. Scale bars 50 µm. (A) Cells phenotypically changed
583 from N-type to S-type by ATRA treatment. (B) Relatively greater number of differentiated cells
584 oriented and aligned on different membranes compared to the naked surface as a negative control.
585 PDL/laminin provided a physiologically optimal environment for neuronal adhesion and expansion.

586 Figure 4. Purification of primary rat RGCs. (A) Retinal cells were isolated and converted into a cell
587 suspension by triturating. The cell suspension was filtered through a mesh filter (>40 µm) to yield a
588 single cell suspension. For magnetic assisted cell sorting (MACS), the single cell suspension was
589 incubated with the RGC-specific marker CD90.1 microbeads and passed through an LS column to hold
590 the micro bead-labelled cells (RGCs) in the magnetic field. The adherent RGCs were rinsed to deplete
591 endothelial cells and microglia. The column was removed from the separator and the adhered cells were
592 flushed out by firmly pushing the plunger into the column and counted. (B) Flow cytometry results
593 showed that CD90.1+ cells were more purified after positive selection using MACS (orang, 70.4%
594 purity) rather than mesh filtration (blue, 37.4%) and initial retinal single-cell suspension (red, 19.8%).

595 Figure 5. CD90.1 immunostaining of isolated rat RGCs by MACS. (A) After 3-day normal culture,
596 RGCs continued to express the specific marker, CD90.1. Nuclear staining was performed using DAPI.
597 (B) The axonal connections were observed between multiple RGCs in the merged image.

598 Figure 6. Schematic of the pressure set-up to simulate glaucomatous condition. A sealed pressure chip
599 inside the incubator was connected to a gauge and regulators placed outside by the polyurethane hoses
600 and pneumatic valves via a side opening in the back of incubator.

601 Figure 7. Cell survival assay under NP* and EP** conditions (Two-way ANOVA, N=4, graphs display
602 mean ±SD). (A) There was a significant decrease over time for untreated cells under EP condition with
603 mean difference (Mean Diff.) =45.35, 56, 51.83, 55.43, and 51.2 at 6, 12, 24, 36 and 48 hours,
604 respectively ($p<0.0001$). (B) BDNF prevented degeneration of treated RGCs under EP condition with

605 Mean Diff. = 20, 22.52, 23.83, 24, and 26.7 at 6, 12, 24, 36 and 48 hours, respectively ($p<0.0001$). (C)
606 RNYK identically protected RGCs under EP condition with Mean Diff. = 26.33, 26.67, 25.67, 26.33,
607 and 27.33 at 6, 12, 24, 36 and 48 hours, respectively ($p<0.0001$).

Figure 1

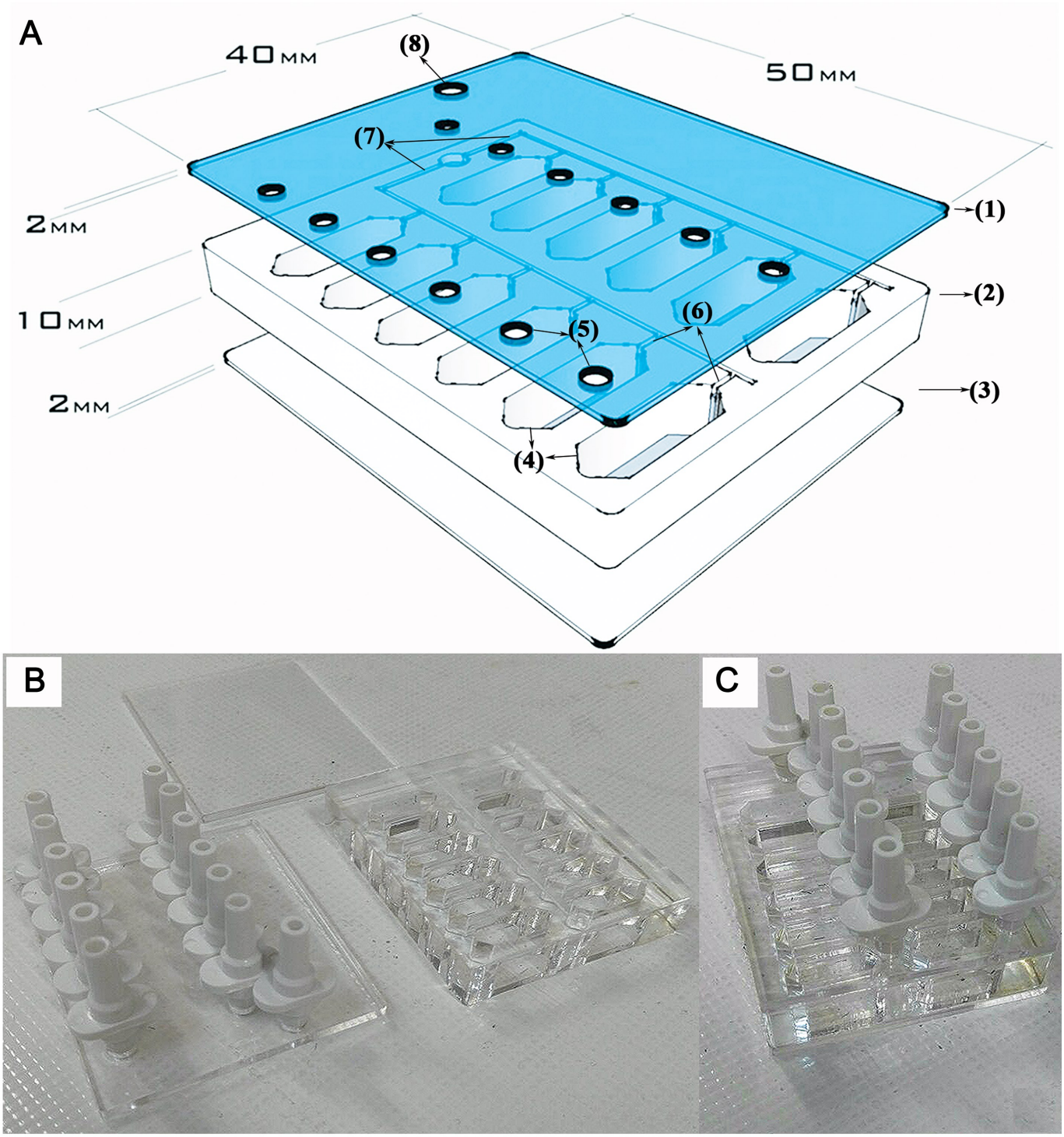

Figure 2

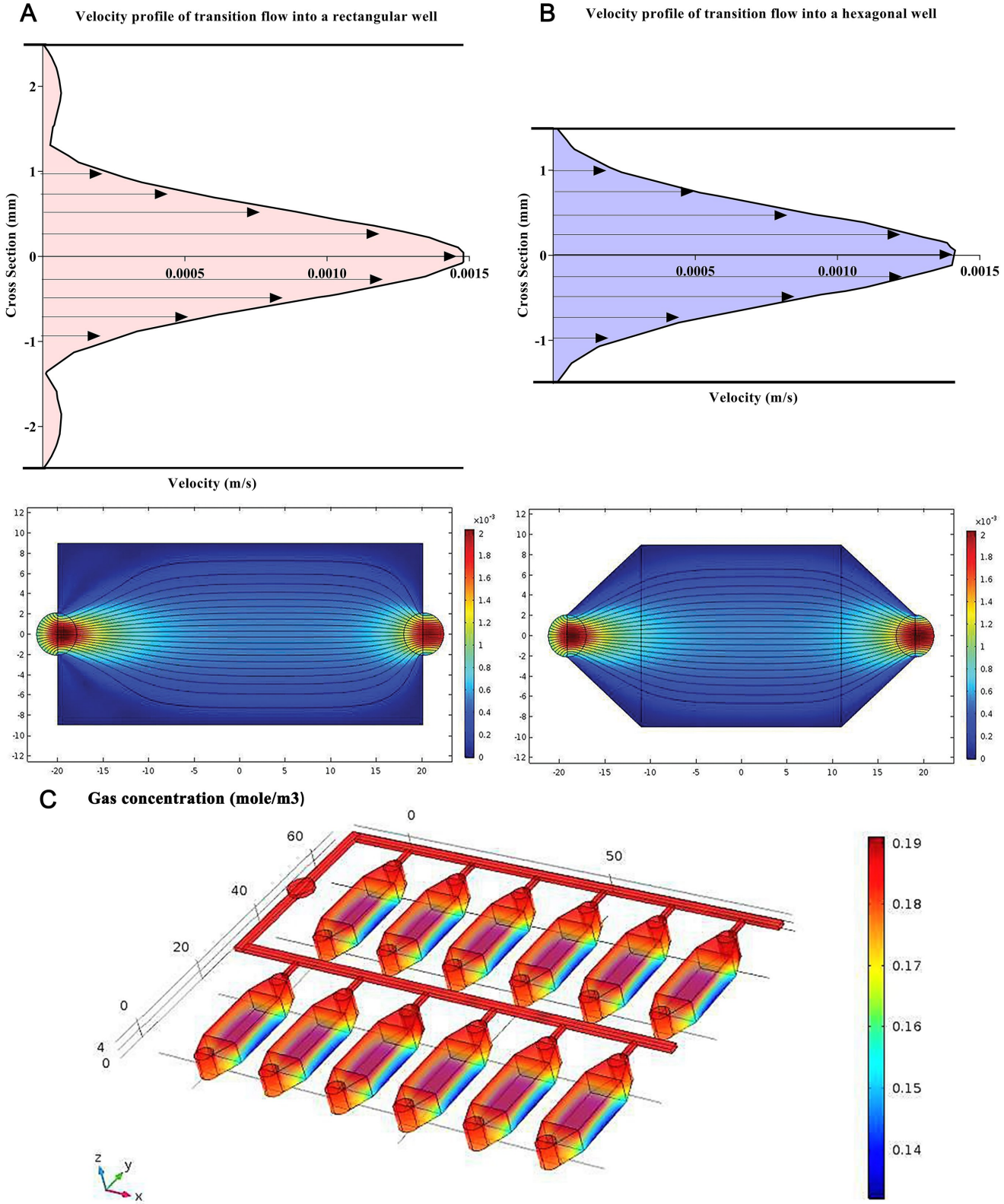
A
Velocity profile of transition flow into a rectangular well
Cross Section (mm)
Velocity (m/s)
0.0005
0.0010
0.0015
B
Velocity profile of transition flow into a hexagonal well
Cross Section (mm)
Velocity (m/s)
0.0005
0.0010
0.0015
C
Gas concentration (mole/m3)
0.19
0.18
0.17
0.16
0.15
0.14

Figure 3

A

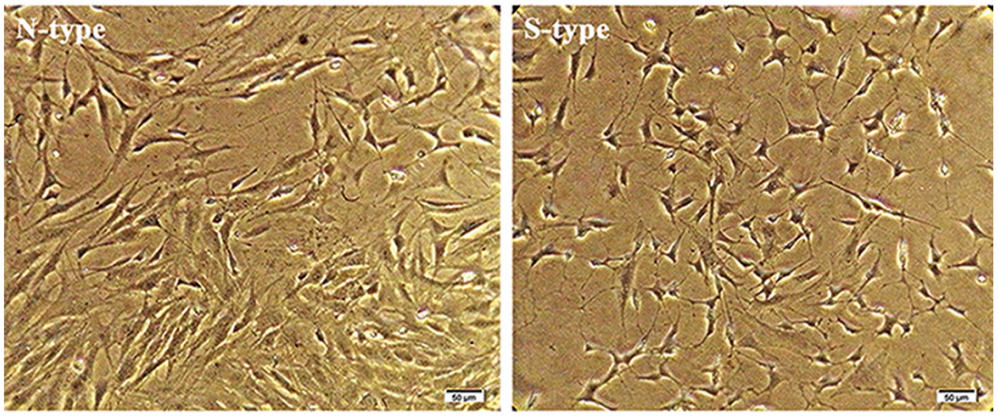
N-type
S-type

B

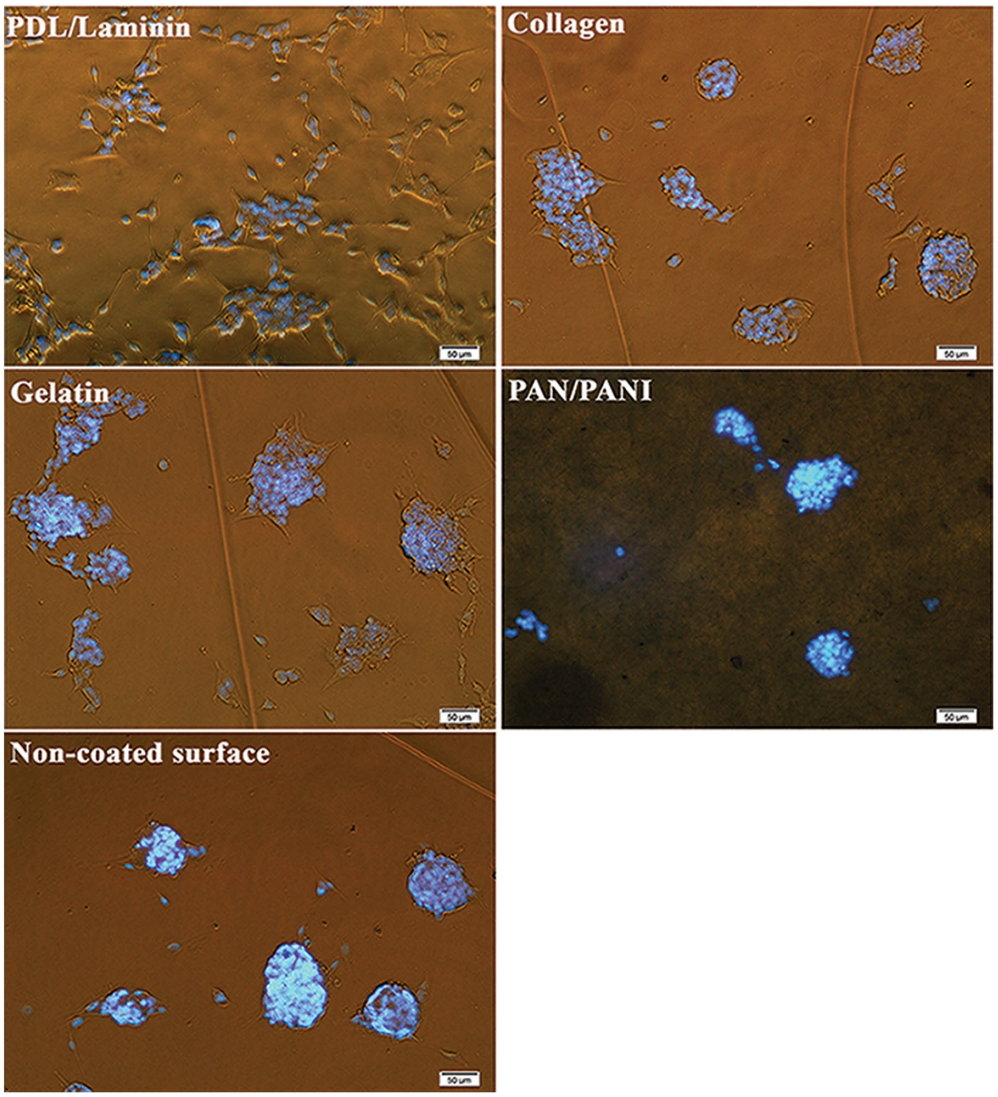
PDL/Laminin
Collagen
Gelatin
PAN/PANI
Non-coated surface

Figure 4

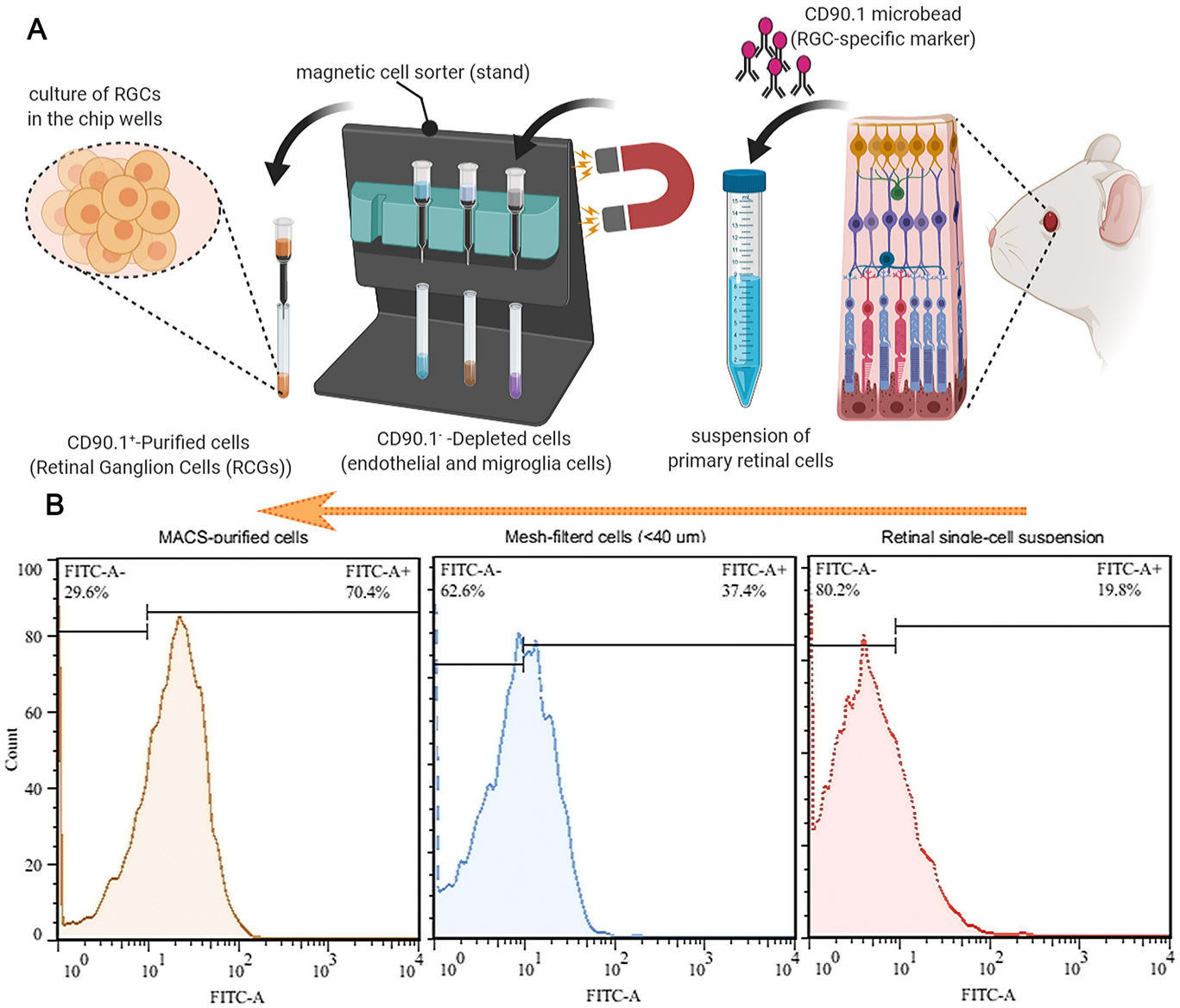
A
CD90.1 microbead
(RGC-specific marker)
magnetic cell sorter (stand)
culture of RGCs
in the chip wells
CD90.1⁺-Purified cells
(Retinal Ganglion Cells (RCGs))
CD90.1⁻ -Depleted cells
(endothelial and migroglia cells)
suspension of
primary retinal cells
B
MACS-purified cells
Mesh-filterd cells (<40 um)
Retinal single-cell suspension
FITC-A-
29.6%
FITC-A+
70.4%
FITC-A-
62.6%
FITC-A+
37.4%
FITC-A-
80.2%
FITC-A+
19.8%
Count
FITC-A

Figure 5

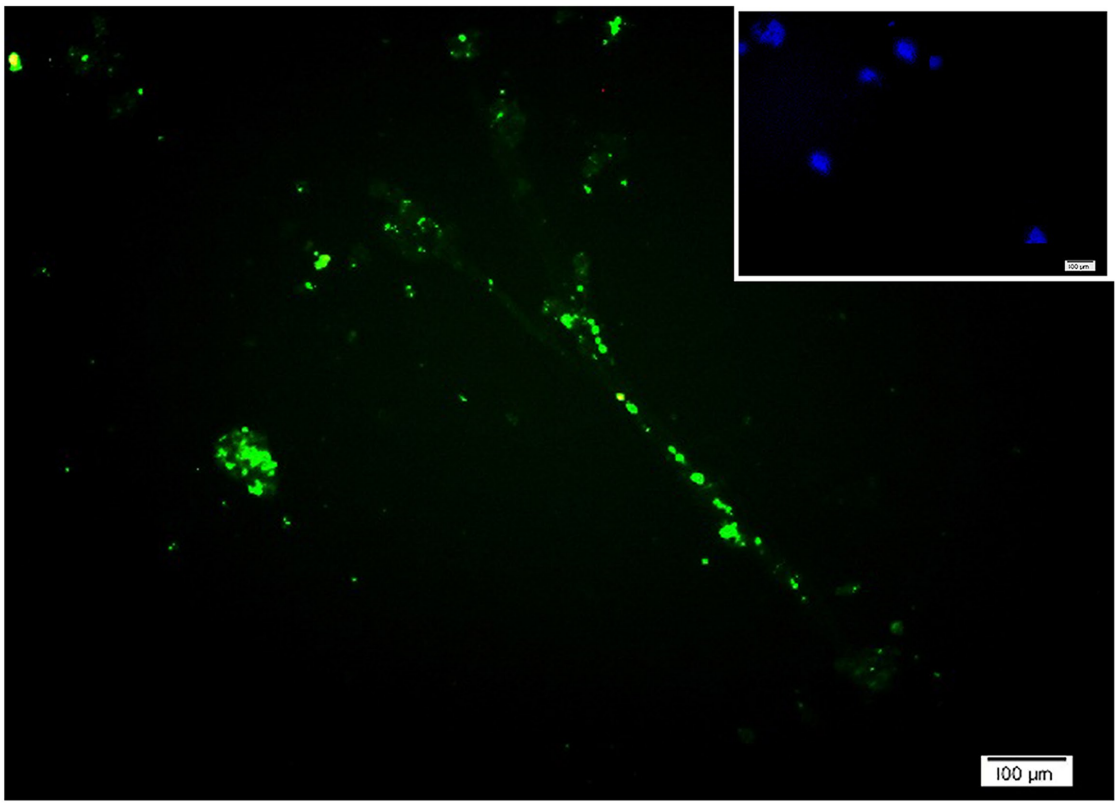

A

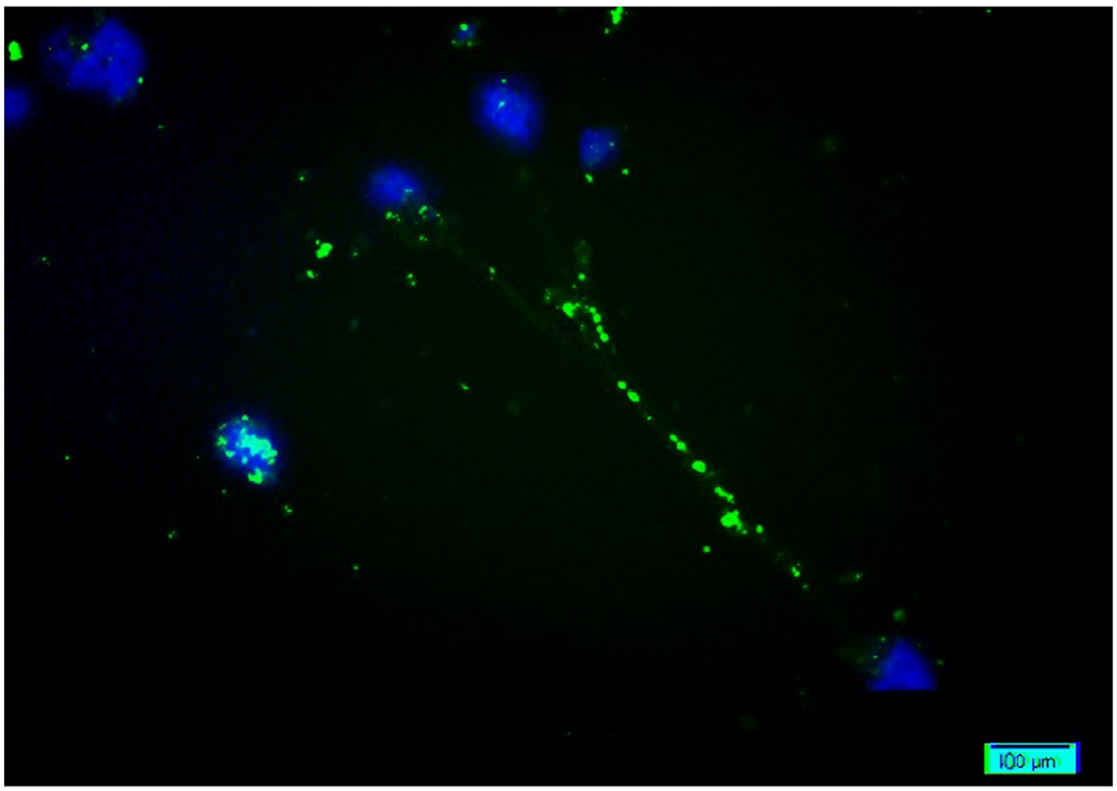

B

Figure 6

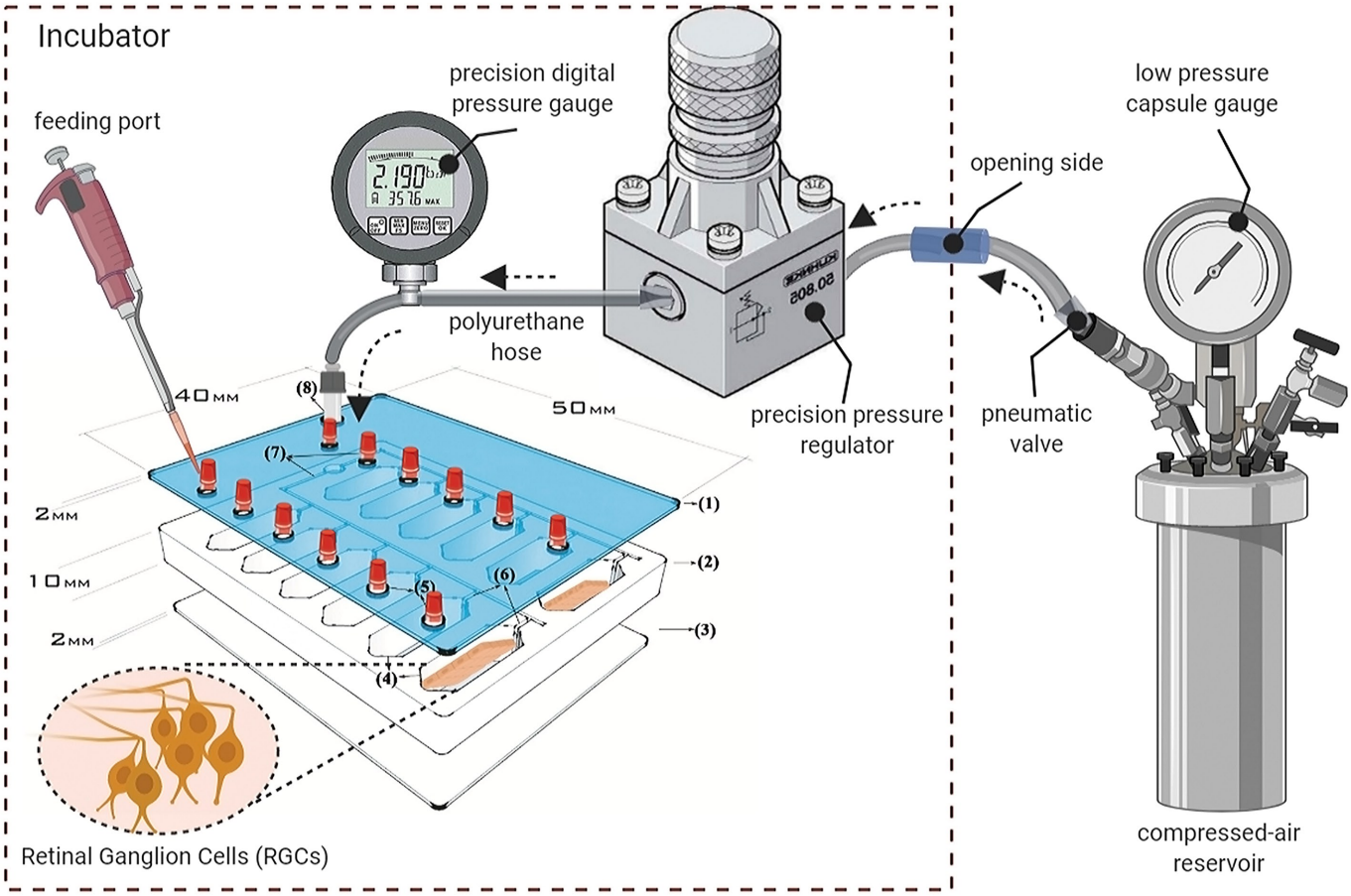
Incubator
feeding port
precision digital pressure gauge
polyurethane hose
precision pressure regulator
opening side
pneumatic valve
low pressure capsule gauge
compressed-air reservoir
40 MM
50 MM
2 MM
10 MM
2 MM
(1)
(2)
(3)
(4)
(5)
(6)
(7)
(8)
Retinal Ganglion Cells (RGCs)

Figure 7

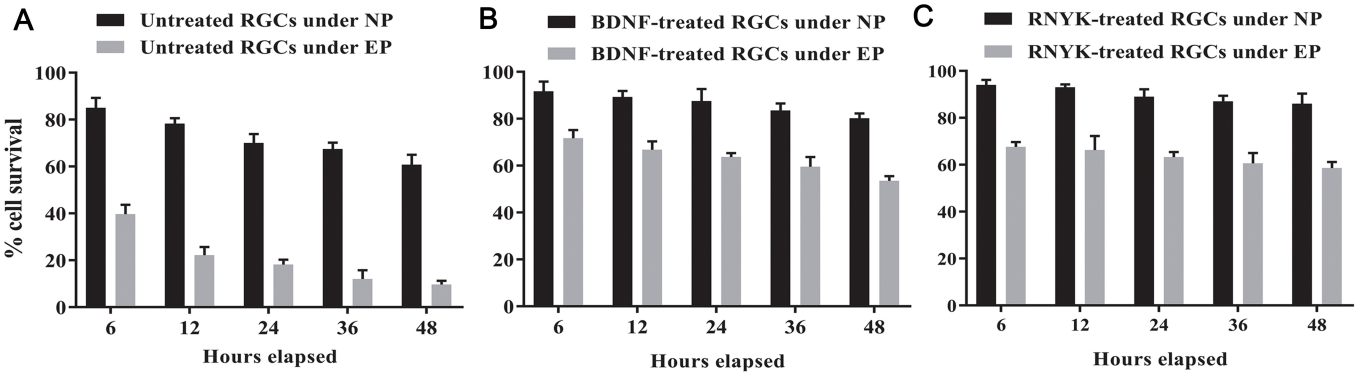
A
Untreated RGCs under NP
Untreated RGCs under EP
% cell survival
100
80
60
40
20
0
6
12
24
36
48
Hours elapsed
B
BDNF-treated RGCs under NP
BDNF-treated RGCs under EP
100
80
60
40
20
0
6
12
24
36
48
Hours elapsed
C
RNYK-treated RGCs under NP
RNYK-treated RGCs under EP
100
80
60
40
20
0
6
12
24
36
48
Hours elapsed